nature nanotechnology

LETTERS

PUBLISHED ONLINE: 2 FEBRUARY 2015 | DOI: 10.1038/NNANO.2014.325

Silicene field-effect transistors operating at room temperature

Li Tao[1], Eugenio Cinquanta[2], Daniele Chiappe[2], Carlo Grazianetti[2], Marco Fanciulli[2], Madan Dubey[3], Alessandro Molle[2]* and Deji Akinwande[1]*

Free-standing silicene, a silicon analogue of graphene, has a buckled honeycomb lattice[1] and, because of its Dirac bandstructure[2,3] combined with its sensitive surface, offers the potential for a widely tunable two-dimensional monolayer, where external fields and interface interactions can be exploited to influence fundamental properties such as bandgap[4] and band character[5] for future nanoelectronic devices[6,7]. The quantum spin Hall effect[3], chiral superconductivity[8], giant magnetoresistance[9] and various exotic field-dependent states[7] have been predicted in monolayer silicene. Despite recent progress regarding the epitaxial synthesis of silicene[8–10] and investigation of its electronic properties[11,13–15], to date there has been no report of experimental silicene devices because of its air stability issue[16]. Here, we report a silicene field-effect transistor, corroborating theoretical expectations regarding its ambipolar Dirac charge transport[17], with a measured room-temperature mobility of ~100 $cm^2 V^{-1} s^{-1}$ attributed to acoustic phonon-limited transport[18] and grain boundary scattering. These results are enabled by a growth–transfer–fabrication process that we have devised—silicene encapsulated delamination with native electrodes. This approach addresses a major challenge for material preservation of silicene during transfer and device fabrication and is applicable to other air-sensitive two-dimensional materials such as germanene[2–4] and phosphorene[19,20]. Silicene's allotropic affinity with bulk silicon and its low-temperature synthesis compared with graphene or alternative two-dimensional semiconductors suggest a more direct integration with ubiquitous semiconductor technology.

The surface sensitivity of silicene derives from its mixed sp^2–sp^3 character[12] and, as such, requires effective passivation or encapsulation at all stages from material synthesis to device fabrication. Although buckled two-dimensional silicon was foreseen two decades ago[1], its instability in air has severely limited investigations of its experimental properties. With this in mind, for the present study on silicene (Fig. 1a) we devised a synthesis–transfer–fabrication process denoted 'silicene encapsulated delamination with native electrodes' (SEDNE) to overcome this challenge. A schematic illustration of the SEDNE process (see Methods) is presented in Fig. 1b, which includes the following key innovations: (1) epitaxial silicene synthesis on deposited Ag(111) thin film on a mica substrate instead of expensive single-crystal bulk Ag, (2) encapsulated delamination transfer of silicene sandwiched between Al_2O_3 and native Ag thin films that enables substrate reuse, unlike the normal wet transfer technique, which sacrifices the growth substrate[21], and (3) reuse of the native Ag film to stabilize the silicene and serve as contact electrodes. Silicene growth on the Ag(111)/mica substrate was monitored by real-time reflection high-energy electron diffraction (RHEED) and *in situ* scanning tunnelling microscopy (STM). When compared to the RHEED pattern of a pristine Ag(111) surface (Fig. 2a), a new set of sub-streaks (Fig. 2b) arising from the silicene are observed. This epitaxial growth leads to a variety of coexisting silicene domains with different periodic order, where the amount depends on the deposition temperature[13,22,23]. Here, despite the multiphase character of the silicene monolayer, two configurations have been selected, which, after careful optimization of the growth conditions, exhibit majority concentrations of the (4×4) and $(\sqrt{13} \times \sqrt{13})$ phases, plus a lesser amount of the $(2\sqrt{3} \times 2\sqrt{3})$ phase[12], which are clearly distinguished by STM (Fig. 2c–e). These phases are consistent with the growth mode and atomistic details of previously reported superstructures of epitaxial silicene monolayer on Ag(111) (obtained by means of atomically resolved microscopy and diffraction)[11,13,15,24,25]. In this Letter, the adopted growth condition is out of the instability regime observed by Acun and co-authors[22].

Raman spectroscopy was used as a routine method to verify the integrity of the silicene on Ag(111). A typical Raman spectrum of silicene is dominated by the presence of a sharp and intense peak in the 515–522 cm^{-1} range, induced by the symmetric stretching of Si–Si atoms in planar hexagons (E_{2g} vibrational modes)[12]. Additionally, the vertical buckling is responsible for the A_{1g} breathing mode, which generates the asymmetric shoulder in the 450–500 cm^{-1} range otherwise absent in bulk sp^3 Si (Supplementary Fig. 1). By comparing Raman spectra as a function of the excitation energy, resonant and non-resonant behaviours can be associated, respectively, with the corresponding superstructures of Ag-supported silicene, which hint at different electronic structures[12,17].

Unlike graphene, exposed silicene is generally unstable in air[16]. This makes it unfeasible to transfer silicene via the widely used wet transfer technique[21], and even Al_2O_3-capped silicene degrades readily once the Ag is removed during transfer (Fig. 3a) because of the exposed bottom surface. Interestingly, we observed that the Raman characteristics of certain silicene phases with Al_2O_3 capping and a native Ag layer appear to be preserved indefinitely (tracked for two months) when stored in a rough vacuum (~30 mbar) at room temperature (Fig. 3b,c). To our knowledge, this is the first experimental evidence supporting density functional theory predictions that *p–d* hybridization of Si–Ag stabilizes silicene grown on Ag(111)[26], and such an interaction could substantially affect the material properties of silicene[5,27]. Therefore, a new encapsulated delamination transfer process was conceived to preserve the silicene–Ag interface during transfer and subsequent device fabrication. The surface morphology (Supplementary Fig. 2) and Raman spectra of silicene–Ag taken 7 days after transfer (Fig. 3d) remain

[1]Microelectronics Research Centre, The University of Texas at Austin, Texas 78758, USA. [2]Laboratorio MDM, IMM-CNR, via C. Olivetti 2, Agrate Brianza, I-20864, Italy. [3]Sensors and Electron Devices Directorate, US Army Research Laboratory, Adelphi, Maryland 20723, USA.
*e-mail: deji@ece.utexas.edu; alessandro.molle@mdm.imm.cnr.it

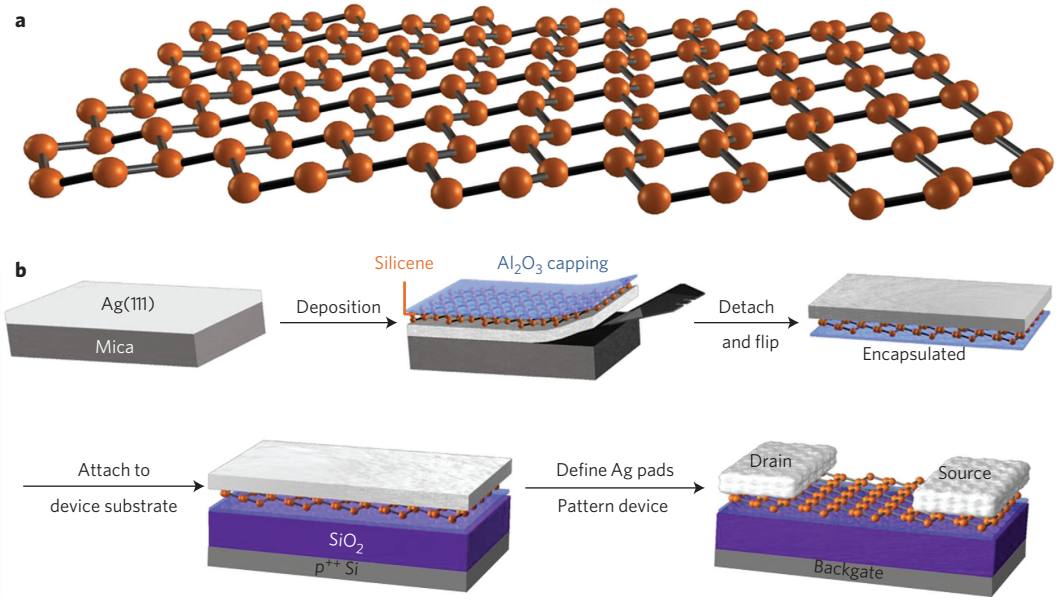

Figure 1 | Schematics of silicene and its synthesis–transfer–fabrication process. a, Buckled honeycomb lattice structure of silicene. **b**, Silicene encapsulated delamination with native electrode (SEDNE) process, which includes the following key steps: epitaxial growth of silicene on crystallized Ag(111) thin film, *in situ* Al_2O_3 capping, encapsulated delamination transfer of silicene, and native contact electrode formation to enable back-gated silicene transistors.

the same as those of the freshly grown sample, indicating that pristine silicene was preserved.

Given the essential role of Si–Ag interaction in stabilizing silicene, device fabrication following the encapsulated delamination transfer of silicene takes an etch-back approach to define source/drain contacts in the native Ag film. To prevent rapid oxidation from the commonly used Ag etchant, we developed a potassium iodide-based iodine-containing solution to etch the Ag without causing damage to the silicene underneath (see Methods). Figure 4a presents a field-effect transistor (FET) with source and drain electrodes defined in the native Ag film at both ends of the silicene channel on $Al_2O_3/SiO_2/p^{++}$ Si substrate. The step profile (Fig. 4b) measured by atomic force microscopy (AFM) indicates a

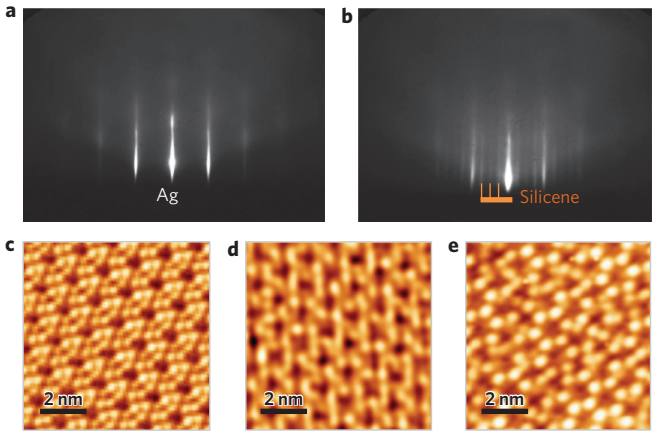

Figure 2 | *In situ* materials characterization of silicene synthesis. a,**b**, Real-time RHEED on Ag(111) (**a**) and silicene on Ag(111) (**b**) (the azimuth is along the [11$\bar{2}$] Ag surface direction and the emergence of extra streaks in the RHEED pattern in **b** results from silicene epitaxy). **c**–**e**, *In situ* scanning tunnelling microscopy (STM) shows three main Si overlayers: (4 × 4) (**c**), ($\sqrt{13} \times \sqrt{13}$) (**d**) and ($2\sqrt{3} \times 2\sqrt{3}$) superstructures (**e**). The STM images are 10 × 10 nm^2 and were acquired with a sample bias of –1.4 V and tunnelling current of 0.5 nA.

channel thickness of ~0.4 nm, consistent with monolayer silicene[28]. Electrostatic transfer and output measurements were subsequently performed using the highly doped silicon substrate as the backgate. In brief, electrical measurements on such silicene transistors under ambient conditions revealed transport behaviour similar to graphene, due to their analogous Dirac bandstructures. A linear drain current output (I_d) to drain voltage (V_d) relation is typically observed in silicene FETs with native Ag electrodes, indicating an ohmic contact under ambient conditions (Fig. 5a). The response curve of I_d or $R = V_d/I_d$ to backgate voltage V_g defines important transistor parameters such as (1) on/off ratio, as the measured maximum over minimum value of I_d (I_{max}/I_{min}) or R (R_{max}/R_{min}), and (2) Dirac voltage (V_{Dirac}) as the gate voltage where R_{max} occurs. The transfer characteristics of several measured FETs (Fig. 5b,c) provide device evidence of silicene's Dirac-like bandstructure. Figure 5b presents R versus gate overdrive voltage ($V_g - V_{Dirac}$) from device 1 (Fig. 5a) on a mixed-phase silicene, which contain ($\sqrt{13} \times \sqrt{13}$) as well as (4 × 4) superstructures. Another transfer characteristic from device 2 on the same mixed-phase silicene is shown in Fig. 5c, with an on/off ratio of about one order of magnitude. Figure 5d shows the V-shape I_d versus V_g curve from device 2, with $V_{Dirac} < |1|$ V, indicating negligible impurity doping as a result of the clean delamination transfer, which is rarely observed in similar backgate FETs made from graphene using an established wet transfer process. By using a well accepted ambipolar diffusive model[29] for graphene FETs, silicene hole and electron mobilities were extracted as 129 and 58 cm^2 V^{-1} s^{-1}, respectively, with a residual carrier concentration (n_o) at the Dirac point of 2.6–7.2 × 10^9 cm^{-2} for device 1. For device 2, the extracted hole and electron mobilities were 99 and 86 cm^2 V^{-1} s^{-1}, respectively, with an n_o of 3.5–7.6 × 10^9 cm^{-2}. A similar ambipolar transfer behaviour applies to silicene FET made from the ($2\sqrt{3} \times 2\sqrt{3}$) phase (Supplementary Fig. 3). The observation of an ambipolar character irrespective of the silicene phase can be rationalized by the predicted bandstructure of silicene, where a Dirac cone is expected from ($\sqrt{13} \times \sqrt{13}$) and ($2\sqrt{3} \times 2\sqrt{3}$) phases after removal of the Ag support[17]. Overall, the mobility values measured for silicene devices are of the order of 100 cm^2 V^{-1} s^{-1}, which is within the estimated range of 10–1,000 cm^2 V^{-1} s^{-1} for supported silicene from

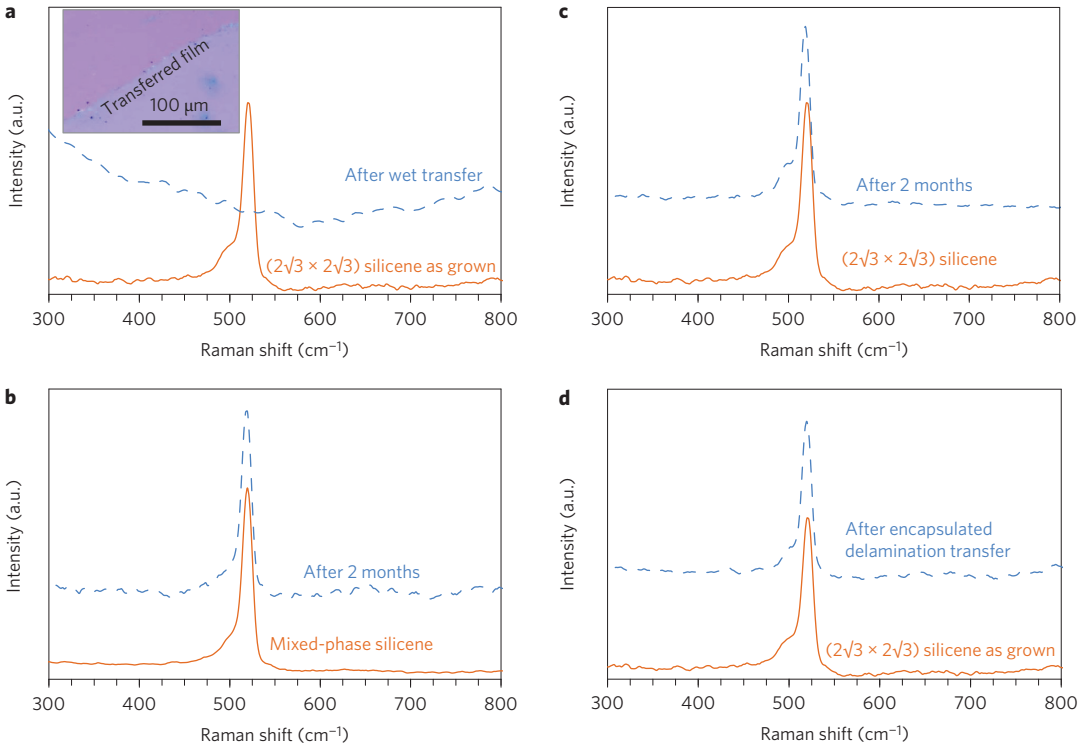

Figure 3 | Monitoring air stability of Ag-supported silicene by Raman spectroscopy. a, Raman spectra of $(2\sqrt{3} \times 2\sqrt{3})$ silicene as grown and after wet transfer. Inset: Silicene film on SiO_2/Si substrate by wet transfer. **b**,**c**, Raman scans on $(\sqrt{13} \times \sqrt{13})$ and (4×4) mixed-phase silicene and $(2\sqrt{3} \times 2\sqrt{3})$ silicene before and after two months of storage in 30 mbar rough vacuum at room temperature. **d**, Raman signatures of $(2\sqrt{3} \times 2\sqrt{3})$ silicene as grown and 7 days after our encapsulated delamination transfer.

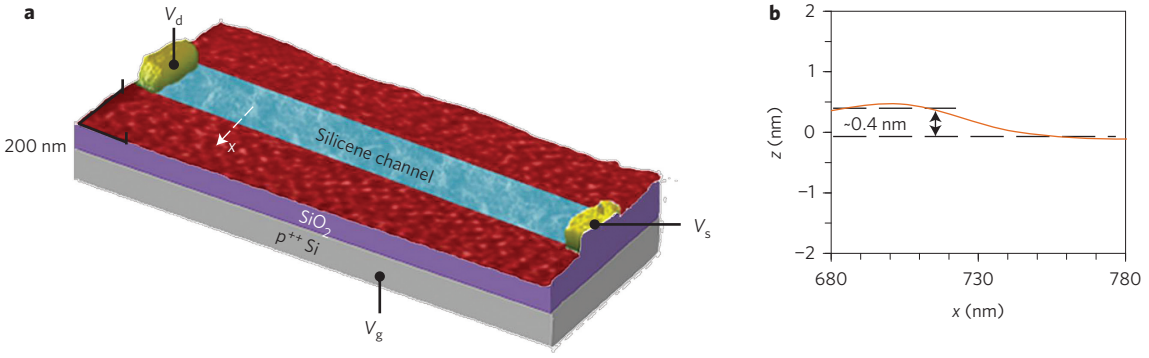

Figure 4 | Silicene FET device. a, Three-dimensional rendering of AFM image on a silicene FET on 90-nm-thick SiO_2/p^{++} Si substrate, including the channel (false-coloured for visual guide) and source/drain contacts (~100-nm-thick) defined in native Ag film. V_g, V_s and V_d are the gate, source and drain voltages, respectively, in electrical measurements. **b**, Cross-sectional height profile, taken along the white dashed line in **a**, indicates a silicene channel thickness of ~0.4 nm.

recent theoretical calculations[18,30]. Control group devices ruled out the possibility of channel current from monolayer amorphous Si or 5-nm Al_2O_3 capping layer (Supplementary Figs 4 and 5). On the other hand, thin Ag residue exhibits a metallic linear current–voltage response (drain current three orders higher than in silicene devices) with no gate modulation (Supplementary Fig. 6). Importantly, the exposed silicene channel loses its Raman and electrical signatures in ~2 min in air, probably as a result of degrading to an amorphous insulator (Supplementary Fig. 7). Hence, we can conclude that the observed ambipolar character in Fig. 5 is indeed from the silicene channel (Supplementary Table 1).

New insights can also be gained from the room-temperate silicene transistor response. Notably, the residual carrier concentration, n_o, of silicene FETs is more than an order of magnitude lower than that of pristine graphene ($\sim 1.5 \times 10^{11}$ cm^{-2}) at 20 °C (ref. 31), which, combined with the $\geq 10 \times I_{max}/I_{min}$ ratio (larger than typical graphene FETs, ~5×)[21,29], suggests that a small bandgap opening is present in our fabricated silicene FETs on $Al_2O_3/SiO_2/p^{++}$ Si substrate. We recall here that the thermally generated n_o of a Dirac semiconductor with zero bandgap has one material dependency, the Fermi velocity (v_F), where $n_o \propto (1/v_F^2)$ (ref. 31). Because the Fermi velocity of silicene is comparable to graphene[15,18], the most plausible scenario to understand silicene's low n_o necessitates a small bandgap opening. In the limit of a weak perturbation to the Dirac dispersion of Ag-free silicene, the small bandgap that yields $n_o \approx 8 \times 10^9$ cm^{-2} is calculated to be ~210 meV (Supplementary equations (1) and (2)), an approximate value and, in principle, consistent with fundamental studies on the band sensitivity of silicene

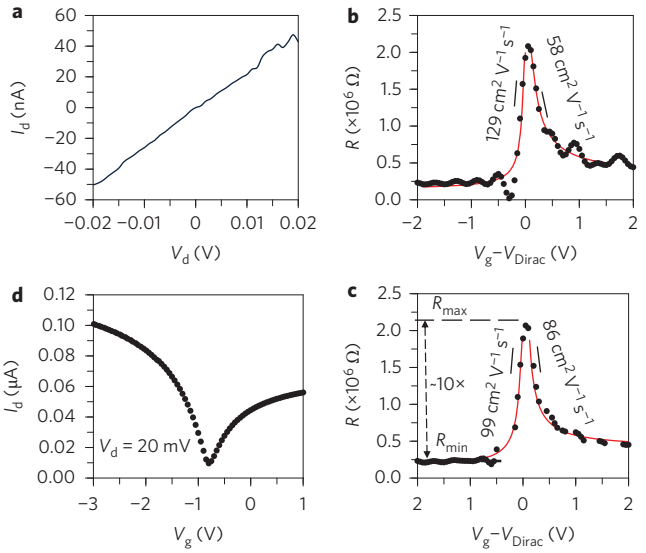

Figure 5 | Room-temperature electrical characterization of silicene transistor devices. a, Low-field linear I_d versus V_d response at $V_g = 0$. **b**,**c**, R versus (V_g–V_{dirac}) of silicene devices 1 and 2, respectively. Measured transfer characteristics (dots) are in good agreement with a widely used ambipolar diffusive transport model[29] (line), which yields extracted low-field hole and electron carrier mobilities of 129 and 99 $cm^2 V^{-1} s^{-1}$ and 58 and 86 $cm^2 V^{-1} s^{-1}$ in devices 1 and 2, respectively, with similar residual carrier concentration of ~3–7 × $10^9 cm^{-2}$, more than an order of magnitude lower than in graphene transistors. **d**, I_d versus V_g curve of silicene device 2 displays ambipolar electron–hole symmetry expected from silicene[2,15]. In **b**–**d**, both devices are from the same mixed-phase silicene sample, with channel length of 1.8 μm and width of 230 nm, and fixed $V_d = 20$ mV for the measurements.

to interfaces[5,27,32,33]. In light of our SEDNE process, further experimental studies are now feasible to elucidate the bandgap dependence of silicene on a variety of substrates.

Furthermore, the mobility values of the experimental silicene transistors are significantly lower than graphene given the same device configuration. Although some scattering mechanisms such as remote phonon, charged impurity and disorders are common to graphene and silicene synthesized two-dimensional materials, a principal mechanism responsible for the observed low mobility is understood to originate from the strong acoustic phonon scattering present in silicene[18]. Unlike planar graphene, with its intrinsic reflection symmetry that suppresses out-of-plane acoustic (ZA) phonons, silicene's buckled structure breaks such symmetry with respect to the atomic plane, resulting in particularly strong ZA phonon scattering[18]. Although pristine free-standing silicene is predicted to offer an intrinsic mobility of ~1,000 $cm^2 V^{-1} s^{-1}$ (ref. 18), the substrate effect on silicene's acoustic phonon energies and electron–phonon coupling is probably perturbed negatively in our experimental studies across several separate transistor devices. Further experimental investigation is warranted to shed light on the upper mobility limit that can be achieved on common and optimized dielectric substrates. Another important charge transport topic that requires more device studies is grain boundary scattering in silicene, which can strongly impact mobility, particularly in mixed-phase films. This topic has been well studied in graphene monolayers[34], but remains to be explored in silicene.

In summary, silicene was grown on Ag(111) film on mica and verified via *in situ* characterizations. Encapsulated delamination transfer and native Ag contact were developed as key innovations, preserving the silicene during transfer for device fabrication and measurements, and allowing the reuse of growth substrates. To our knowledge, this work demonstrates the first proof-of-concept silicene device that is in agreement with predictions of Dirac-like ambipolar charge transport. The low residual carrier density and high gate modulation compared with graphene suggest a small bandgap opening in the experimental devices. The carrier mobility was ~100 $cm^2 V^{-1} s^{-1}$ for these initial devices, with future research on interface engineering likely to be promising avenues for tuning the bandstructure and enhancing the charge transport. Importantly, our encapsulated delamination concept paves the path to carrying out experimental fundamental and device research on silicene, a hitherto outstanding challenge. Moreover, silicene can now be considered a feasible two-dimensional nanomaterial beyond graphene, with the added value of being inherently compatible with ubiquitous silicon semiconductor technology.

Methods

Silicene synthesis and characterization. Material synthesis was performed in a system including an ultrahigh-vacuum chamber at a base pressure of 10^{-10}–10^{-11} mbar (7.5×10^{-11}–10^{-12} torr), with three interconnected chambers for sample processing, chemical analysis and *in situ* STM characterization. Several cycles of Ar^+ ion sputtering (1 keV) were first performed on the Ag(111)/mica substrate to reveal a clean surface, followed by annealing at 530 °C for 30 min. Silicene film was deposited on the processed Ag(111) surface from a heated crucible in the built-in evaporator at a temperature of 250–270 °C and a rate of 2–6 × 10^{-2} monolayers per minute. *In situ* RHEED (30 keV) and STM (sample bias of −1.4 V and tunnelling current of 0.5 nA) were used to monitor the real-time growth and phase characterization. A non-reactive *in situ* capping procedure[16] was adopted to protect epitaxial silicene on Ag(111) by means of reactive molecular beam deposition of Al_2O_3 with a thickness of 5 nm. Raman spectroscopy was performed in a Renishaw In-via spectrometer with a 442 nm (2.81 eV) He-Cd blue laser at 4 mW power. The surface morphology of the transferred silicene and the fabricated device was measured by a Veeco Digital Instrument AFM in tapping mode.

Transfer, device fabrication and characterization. As shown in Fig. 1b, an encapsulated delamination transfer was used to transfer silicene film from a mica growth substrate to the device substrate. A blade (or tape) initiated a gap at the edge of the sample between the Ag and mica interface, allowing the Al_2O_3/silicene/Ag film stack to be peeled off. The encapsulated silicene (between Al_2O_3 and Ag) was then placed on a device substrate (90-nm-thick SiO_2 on p^{++} Si) with the Al_2O_3 layer facing downward in contact with the SiO_2 layer. The silicene channel as well as source/drain electrodes (in native Ag catalyst film) were patterned using electron-beam lithography followed by etching to produce backgate transistor devices. To prevent rapid degradation/oxidation of silicene (as observed with commonly used Ag etchants such as nitric acid), a potassium iodide- and iodine-based etchant was developed in house (Supplementary Section 2). This provides a short but sufficient time window to capture the charge transportation behaviour in Ag-free silicene before its degradation in ~2 min in air (Supplementary Fig. 7). With this in mind, the fabricated back-gated transistor device was measured immediately on a Cascade or Lakeshore probe station with an Agilent 4156 analyser using $V_d = 20$ mV with V_g swept from −2 to 2 V under ambient conditions. A well accepted ambipolar graphene FET diffusive model[29] was used to extract the field-effect mobility and residual carrier density from the I_d versus V_g measurement data.

Received 10 July 2014; accepted 10 December 2014; published online 2 February 2015

References

1. Takeda, K. & Shiraishi, K. Theoretical possibility of stage corrugation in Si and Ge analogs of graphite. *Phys. Rev. B* **50,** 14916–14922 (1994).
2. Cahangirov, S., Topsakal, M., Aktürk, E., Şahin, H. & Ciraci, S. Two- and one-dimensional honeycomb structures of silicon and germanium. *Phys. Rev. Lett.* **102,** 236804 (2009).
3. Liu, C-C., Feng, W. & Yao, Y. Quantum spin Hall effect in silicene and two-dimensional germanium. *Phys. Rev. Lett.* **107,** 076802 (2011).
4. Ni, Z. *et al.* Tunable bandgap in silicene and germanene. *Nano Lett.* **12,** 113–118 (2011).
5. Lin, C-L. *et al.* Substrate-induced symmetry breaking in silicene. *Phys. Rev. Lett.* **110,** 076801 (2013).
6. De Padova, P. *et al.* 1D graphene-like silicon systems: silicene nano-ribbons. *J. Phys. Condens. Matter* **24,** 223001 (2012).
7. Ezawa, M. Valley-polarized metals and quantum anomalous Hall effect in silicene. *Phys. Rev. Lett.* **109,** 055502 (2012).
8. Liu, F., Liu, C-C., Wu, K., Yang, F. & Yao, Y. *d+id'* chiral superconductivity in bilayer silicene. *Phys. Rev. Lett.* **111,** 066804 (2013).
9. Xu, C. *et al.* Giant magnetoresistance in silicene nanoribbons. *Nanoscale* **4,** 3111–3117 (2012).

10. Aufray, B. *et al.* Graphene-like silicon nanoribbons on Ag(110): a possible formation of silicene. *Appl. Phys. Lett.* **96,** 183102 (2010).
11. Feng, B. *et al.* Evidence of silicene in honeycomb structures of silicon on Ag(111). *Nano Lett.* **12,** 3507–3511 (2012).
12. Cinquanta, E. *et al.* Getting through the nature of silicene: an sp^2–sp^3 two-dimensional silicon nanosheet. *J. Phys. Chem. C* **117,** 16719–16724 (2013).
13. Chiappe, D., Grazianetti, C., Tallarida, G., Fanciulli, M. & Molle, A. Local electronic properties of corrugated silicene phases. *Adv. Mater.* **24,** 5088–5093 (2012).
14. De Padova, P. *et al.* Multilayer silicene nanoribbons. *Nano Lett.* **12,** 5500–5503 (2012).
15. Vogt, P. *et al.* Silicene: compelling experimental evidence for graphenelike two-dimensional silicon. *Phys. Rev. Lett.* **108,** 155501 (2012).
16. Molle, A. *et al.* Hindering the oxidation of silicene with non-reactive encapsulation. *Adv. Funct. Mater.* **23,** 4340–4344 (2013).
17. Scalise, E. *et al.* Vibrational properties of epitaxial silicene layers on (111) Ag. *Appl. Surf. Sci.* **291,** 113–117 (2014).
18. Li, X. *et al.* Intrinsic electrical transport properties of monolayer silicene and MoS_2 from first principles. *Phys. Rev. B* **87,** 115418 (2013).
19. Li, L. *et al.* Black phosphorus field-effect transistors. *Nature Nanotech.* **9,** 372–377 (2014).
20. Liu, H. *et al.* Phosphorene: an unexplored 2D semiconductor with a high hole mobility. *ACS Nano* **8,** 4033–4041 (2014).
21. Piner, R. *et al.* Graphene synthesis via magnetic inductive heating of copper substrates. *ACS Nano* **7,** 7495–7499 (2013).
22. Acun, A., Poelsema, B., Zandvliet, H. J. W. & van Gastel, R. The instability of silicene on Ag(111). *Appl. Phys. Lett.* **103,** 263119 (2013).
23. Moras, P., Mentes, T. O., Sheverdyaeva, P. M., Locatelli, A. & Carbone, C. Coexistence of multiple silicene phases in silicon grown on Ag(111). *J. Phys. Condens. Matter* **26,** 185001 (2014).
24. Mannix, A. J., Kiraly, B., Fisher, B. L., Hersam, M. C. & Guisinger, N. P. Silicon growth at the two-dimensional limit on Ag(111). *ACS Nano* **8,** 7538–7547 (2014).
25. Lin, C-L. *et al.* Structure of silicene grown on Ag(111). *Appl. Phys. Exp.* **5,** 045802 (2012).
26. Gao, J. & Zhao, J. Initial geometries, interaction mechanism and high stability of silicene on Ag(111) surface. *Sci. Rep.* **2,** 861 (2012).
27. Guo, Z-X., Furuya, S., Iwata, J-I. & Oshiyama, A. Absence and presence of Dirac electrons in silicene on substrates. *Phys. Rev. B* **87,** 235435 (2013).
28. Resta, A. *et al.* Atomic structures of silicene layers grown on Ag(111): scanning tunneling microscopy and noncontact atomic force microscopy observations. *Sci. Rep.* **3,** 2399 (2013).
29. Kim, S. *et al.* Realization of a high mobility dual-gated graphene field-effect transistor with Al_2O_3 dielectric. *Appl. Phys. Lett.* **94,** 062107–062103 (2009).
30. Wang, R. *et al.* Silicene oxides: formation, structures and electronic properties. *Sci. Rep.* **3,** 3507 (2013).
31. Wong, H-S. P. & Akinwande, D. *Carbon Nanotube and Graphene Device Physics* (Cambridge Univ. Press, 2011).
32. Cahangirov, S. *et al.* Electronic structure of silicene on Ag(111): strong hybridization effects. *Phys. Rev. B* **88,** 035432 (2013).
33. Tsoutsou, D., Xenogiannopoulou, E., Golias, E., Tsipas, P. & Dimoulas, A. Evidence for hybrid surface metallic band in (4×4) silicene on Ag(111). *Appl. Phys. Lett.* **103,** 231604 (2013).
34. Tsen, A. W. *et al.* Tailoring electrical transport across grain boundaries in polycrystalline graphene. *Science* **336,** 1143–1146 (2012).

Acknowledgements

This work is supported in part by the Army Research Office (contract W911NF-13-1-0364), the Southwest Academy of Nanoelectronics (SWAN) centre sponsored by the Semiconductor Research Corporation (SRC) and the Future and Emerging Technologies (FET) programme within the Seventh Framework Program for Research of the European Commission (FET-Open grant number 270749, '2D-Nanolattices' project). D.A. acknowledges the TI/Jack Kilby Faculty Fellowship. The authors thank A. Nayak and J. Wozniak of Texas Advanced Computing Centre (TACC) for their help with the three-dimensional rendering of Figure 1.

Author contributions

E.C., D.C. and C.G. performed epitaxial growth of silicene with *in situ* RHEED and STM characterization. L.T. and E.C. conducted Raman spectroscopy studies on silicene stability. L.T., with D.A., devised and conducted the silicene transfer, device fabrication, transport measurements and analysis of device data. M.F. and A.M. managed the technical resources at the Laboratorio MDM, National Research Council (CNR) – Institute for Microelectronics and Microsystems (IMM), Italy. All authors contributed to the writing based on the draft written by L.T. and D.A. D.A. and A.M. coordinated and supervised the research.

Additional information

Supplementary information is available in the online version of the paper. Reprints and permissions information is available online at www.nature.com/reprints. Correspondence and requests for materials should be addressed to A.M. and D.A.

Competing financial interests

The authors declare no competing financial interests.